Received: 9 May 2023 | Revised: 19 June 2023 | Accepted: 28 June 2023

DOI: 10.1002/cey2.433

RESEARCH ARTICLE

CARBON ENERGY WILEY

Understanding the correlation between energy-state mismatching and open-circuit voltage loss in bulk heterojunction solar cells

Hyun-Seock Yang[1,2] | **Danbi Kim**[1,3] | **Chang-Mok Oh**[4] | **Vellaiappillai Tamilavan**[1,3] | **Pesi M. Hangoma**[1,3] | **Hojun Yi**[1,3] | **Bo R. Lee**[1,3] | **Insoo Shin**[5] | **In-Wook Hwang**[4] | **Sung Heum Park**[1,3]

[1]Pukyong National University, Busan, Republic of Korea

[2]Clarendon Laboratory, University of Oxford, Oxford, UK

[3]Institute of Energy Transport and Fusion Research, Pukyong National University, Busan, Republic of Korea

[4]Advanced Photonics Research Institute, Gwangju Institute of Science and Technology, Gwangju, Republic of Korea

[5]Department of Chemical and Biomolecular Engineering, Tandon School of Engineering, New York University, Brooklyn, New York, USA

Correspondence

Insoo Shin, Department of Chemical and Biomolecular Engineering, Tandon School of Engineering, New York University, Brooklyn, NY 11201 USA.
Email: is2708@nyu.edu

In-Wook Hwang, Advanced Photonics Research Institute, Gwangju Institute of Science and Technology, 61005 Gwangju, Republic of Korea.
Email: hwangiw@gist.ac.kr

Sung Heum Park, Pukyong National University, 45, Yongso-ro, Nam-gu, Busan 48513, Republic of Korea.
Email: spark@pknu.ac.kr

Funding information

National Research Foundation of Korea, Grant/Award Number: 2022R1A6A1A03051158; BrainLink Program, Grant/Award Number: 2022H1D3A3A01077343; Nano Material Technology Development Program, Grant/Award Number: 2021M3H4A1A02057007

Abstract

Photoinduced intermolecular charge transfer (PICT) determines the voltage loss in bulk heterojunction (BHJ) organic photovoltaics (OPVs), and this voltage loss can be minimized by inducing efficient PICT, which requires energy-state matching between the donor and acceptor at the BHJ interfaces. Thus, both geometrically and energetically accessible delocalized state matching at the hot energy level is crucial for achieving efficient PICT. In this study, an effective method for quantifying the hot state matching of OPVs was developed. The degree of energy-state matching between the electron donor and acceptor at BHJ interfaces was quantified using a mismatching factor (MF) calculated from the modified optical density of the BHJ. Furthermore, the correlation between the open-circuit voltage (V_{oc}) of the OPV device and energy-state matching at the BHJ interface was investigated using the calculated MF. The OPVs with small absolute MF values exhibited high V_{oc} values. This result clearly indicates that the energy-state matching between the donor and acceptor is crucial for achieving a high V_{oc} in OPVs. Because the MF indicates the degree of energy-state matching, which is a critical factor for suppressing energy loss, it can be used to estimate the V_{oc} loss in OPVs.

KEYWORDS

bulk heterojunction, open circuit voltage, organic photovoltaics, photoinduced charge transfer, voltage loss

1 | INTRODUCTION

The open-circuit voltage (V_{oc}) in organic photovoltaics (OPVs), based on bulk heterojunctions (BHJs) of electron-donating conjugated polymers and electron-accepting materials, is an important parameter for determining power conversion efficiency (PCE).[1–4] To date, researchers have attempted to increase V_{oc} through various approaches, including the use of electron donors with deep highest occupied molecular orbital (HOMO) levels and electron acceptors with shallow lowest unoccupied molecular orbital (LUMO) levels, and inserting a functional layer between the active layer and electrodes. However, the V_{oc} values exhibited by OPVs are still lower than those shown by inorganic semiconductors and perovskite-based photovoltaics.[5–10]

The relatively low V_{oc} of OPVs is mainly ascribed to their large voltage loss, which is induced by a significant photon energy loss in the lowest-lying charge transfer (CT) states that are located deeper than the LUMO of the electron acceptor.[11] Because a substantial number of electrons and holes separated at the interface undergo nonradiative recombination in the lowest-lying CT states, inefficient photoinduced charge transfer (PICT) occurs in the vicinity of the LUMO level of the electron acceptor, resulting in a loss of V_{oc}.[12–17] According to a previous study, efficient PICT for directly generated mobile carriers, without trapping in CT states, could be achieved via hot-state CTs between the electron donors and acceptors.[18] Jakowetz et al.[19] reported that efficient PICT occurs through hot-state charge delocalization between donors and acceptors. They also demonstrated that both geometrically and energetically accessible delocalized state matching is essential for suppressing V_{oc} loss.[19] According to these observations, it is expected that hot-state matching between an electron donor and acceptor is a critical factor for achieving efficient PICT. In addition, ensuring the well-matching of hot states between an electron donor and acceptor is essential for achieving a high V_{oc}. These factors have motivated research to gain an in-depth understanding of hot-state matching between electron donors and acceptors. Although simulations and experimental studies have been performed to investigate hot-state matching between electron donors and acceptors for efficient PICT, systematic studies on the correlation between hot-state matching and V_{oc} loss in actual devices have not been conducted.[20,21] Moreover, because useful methods to quantify hot-state matching involving the LUMO level, as well as a broad range of electronic energy levels between electron donor and acceptor materials, have not been developed, applying hot-state matching to increase V_{oc} in actual devices remains a challenge.

Thus, in this study, the correlation between V_{oc} and hot-state matching in OPVs was investigated by developing an effective method to quantify the degree of hot-state matching between the donor and acceptor. The hot-state matching of the BHJ thin film was analyzed using modified optical density (MOD), which represents the sum of the absorbed photon energy and HOMO level of the material. By analyzing the modified optical density overlapping (MODO) in the BHJ, we calculated the mismatching factor (MF) to quantify the degree of energy-state matching between the electron donors and acceptors at the BHJ interface. The results indicate that a large MF causes a large V_{oc} loss for both binary and ternary OPVs. Finally, we achieved a high-efficiency ternary OPV device with a PCE of 16.15% by controlling the MF between the donor and acceptor.

2 | EXPERIMENTAL SECTION

2.1 | Device fabrication

Indium tin oxide-coated glass substrates were sequentially cleaned in an ultrasonic bath with deionized water, acetone, ethanol, and isopropanol for 10 min and then dried in the oven at 100°C for overnight. The surface of the substrates was then treated with ultraviolet (UV)/ozone treatment for 1800 s; thereafter, poly(3,4-ethylenedioxythiophene)-poly(styrene sulfonate) (PEDOT:PSS; Paytron PH) was spin-coated onto the substrate at the 4500 rpm for 50 s and annealed at 140°C for 10 min. A polymer blend of electron donor (P1, P2, PTB7-Th, and PBDB-T) and electron acceptor ($PC_{71}BM$, ITIC, and IEICO-4F) at various ratios was dissolved in a solution (chlorobenzene:1,8-diiodooctane = 97:3, volume ratio) and thereafter spin-coated on top of the PEDOT/PSS layer. Specifically, the D18:Y6:phenyl-C61-butyric acid methyl ester (PCBM) blend was dissolved in a solution (chloroform:1-chloronaphthalene = 99:1, volume ratio). After coating the active layer, it was washed with 0.2 mL methanol via spin-coating at 3000 rpm for 30 s. Lastly, 100-nm-thick Al electrode was deposited by thermal evaporation in the vacuum of approximately 3×10^{-6} Torr.

2.2 | Characterization

The UV–visible (UV-vis) absorption spectra of conjugated polymer and small molecule materials were measured by using a T70 + UV/vis spectrometer. The saturated V_{oc} and light intensity-dependent V_{oc} were

measured under monochromatic light by using a xenon lamp (Dongwoo Optron). The irradiated current density–voltage (J–V) curves were tested using Keithley 2400 SourceMeter under air mass 1.5 global (AM 1.5G) irradiation (100 mW cm^{-2}). The light intensity was calibrated using the NREL-Si solar cell.

3 | RESULTS AND DISCUSSION

3.1 | Definition of MODO and MF

Hot-state matching between the donor and acceptor in the BHJ is an important factor for increasing the rate of efficiency of PICT, which reduces V_{oc} loss in OPV devices.[18–22] Because the generated electrons move from the electron donor to the electron acceptor at the interface via PICT, a well-matched energy state at the interface leads to efficient electron transfer.[23] In this case, the degree of energy-state overlap between the donor and acceptor at the hot-energy level significantly affects the PICT efficiency of the BHJ.[19] Figure 1A,B illustrates two possible PICT processes in BHJ systems with mismatched and well-matched donor and acceptor states at their interfaces. In both cases, the electrons in the donor are directly excited to the hot-state level from the HOMO level via the absorption of photon energy (vertical yellow arrows) and then delocalized in the hot states.[24,25] If there are no states with energy levels equal to those of the hot state in the acceptor (Figure 1A), then the excited electron spontaneously relaxes and reaches the thermally stable LUMO of the donor and is subsequently transferred to the LUMO of the acceptor via the CT states.[26] In this case, because of the existence of a large number of CT states at levels lower than the LUMO level of the acceptor, a large number of electrons

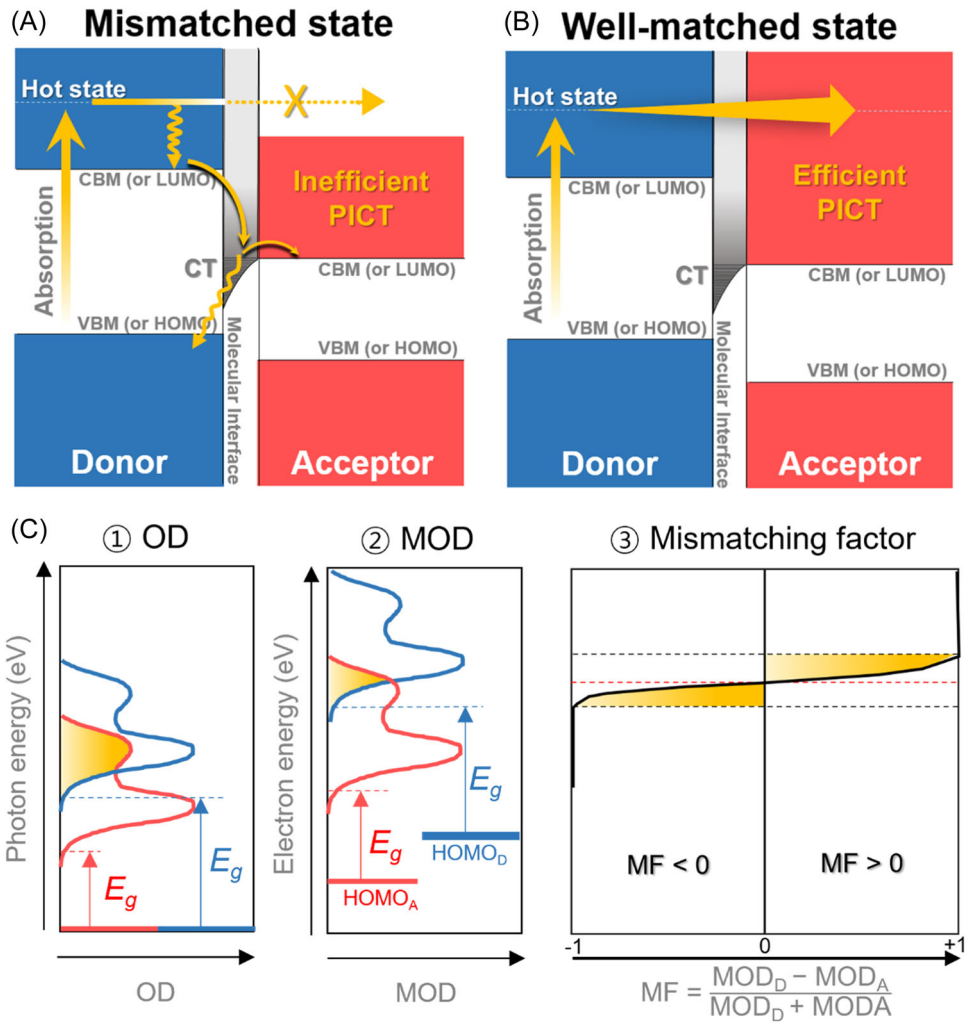

FIGURE 1 Energetics of PICT and hot-state matching of two organic material systems. (A) Mechanism of inefficient PICT at a mismatched state. (B) Mechanism of efficient PICT at a well-matched state. (C) Scheme for determining MF from OD and MOD.

are trapped in the lowest-lying CT states during the transfer process.[27] Because the probability of nonradiative recombination increases in the lowest-lying CT states owing to the Coulomb attractive force between the hole and trapped electron, the trapped electrons are rarely transferred to the mobile carrier state, leading to a significant V_{oc} loss.[24,26–28]

By contrast, the excited electrons in the hot state can be directly transferred to the energy state in the acceptor before relaxation if there are states with energy levels equal to those of the hot state in the acceptor, as shown in Figure 1B.[29–31] In this case, a significantly large number of mobile carriers are generated via the efficient PICT process without trapping in the CT states, leading to a reduced V_{oc} loss.[32] Thus, ensuring energy-state matching at the BHJ interface is crucial for realizing efficient PICT. Developing effective methods for identifying the degree of state matching in a BHJ is crucial for achieving high-performance OPVs with maximum V_{oc}. Although the importance of hot-state matching has been indicated in numerous studies,[11,20] no method for quantifying and visualizing the state matching has been reported. Therefore, we developed a simple and effective method for quantifying and visualizing hot-state matching to ensure efficient PICT.

Figure 1C illustrates the method developed for quantifying and visualizing hot-state matching. We calculated the MF, based on the optical density (OD) and energy-level matching at the donor–acceptor interface, to quantify the degree of energy-state matching. Figure 1C shows ① the pristine OD between the donor and acceptor; the OD spectra of the donor and acceptor were easily obtained by measuring the UV–vis absorption spectra. The red and blue lines indicate the ODs of the acceptor and donor, respectively, and the yellow area represents the area of optical density overlapping (ODO) between the donor and acceptor. In this case, we can easily determine the OD of the state and energy bandgap (E_g) between the valence band maximum (or HOMO level) and conduction band minimum (or LUMO level). However, because ODO does not provide information on the excited electron energy level, estimating hot-state matching using only the ODO information is a challenging task. Therefore, we need additional information on the corresponding energy level of the valence band maximum (or HOMO level) to calculate the energy state of the OD and investigate electron transfer from the donor to the acceptor. Therefore, in this study, we considered the MOD calculated by summing the absorbed photon energy and HOMO levels of each material, as described in Equation (1).

$$E_{\text{excited electron}}(\text{MOD}) = E_{\text{photon}}(\text{OD}) + E_{\text{HOMO}}. \quad (1)$$

To ensure the reliability of the HOMO values, the HOMO values of each material were determined via ultraviolet photoelectron spectroscopy (UPS) measurements. Because the target for the MODO calculation is a thin film, UPS measurements are appropriate to show the exact HOMO level of the thin film.[33] The sum of the absorbed photon energy and HOMO level for each material is depicted in the ② MOD shown in Figure 1C. The yellow area in ① indicates the pristine ODO between the donor and acceptor, whereas the yellow area in ② indicates the MODO. As expected, the overlapping areas of the ODO and MODO significantly differ. Although the shape of each MOD is identical to that of the OD, the degree of overlap between the ODO and MODO significantly differs; this difference originates from the difference between the HOMO levels of the donor and acceptor. Because MOD implies the energy state of the excited electron, the area of the MODO indicates the degree of hot-state matching.

We defined an MF to visualize and quantify the hot-state matching effectively. Fundamentally, the MF is calculated by subtracting the MOD of the acceptor from that of the donor at each electron energy level, as described in Equation (2). The fraction of "$\text{MOD}_{\text{donor}} + \text{MOD}_{\text{accpetor}}$" is the total absorption in the BHJ layer.

$$\text{MF} \equiv \frac{\text{MOD}_{\text{donor}} - \text{MOD}_{\text{acceptor}}}{\text{MOD}_{\text{donor}} + \text{MOD}_{\text{acceptor}}}. \quad (2)$$

As shown in ③ in Figure 1C, a positive MF value indicates "$\text{MOD}_{\text{donor}} > \text{MOD}_{\text{acceptor}}$" at the corresponding energy level, whereas a negative MF value indicates "$\text{MOD}_{\text{donor}} < \text{MOD}_{\text{acceptor}}$." An MF value of zero (red dash line) indicates "$\text{MOD}_{\text{donor}} = \text{MOD}_{\text{acceptor}}$," suggesting well-matched hot energy levels. For the range in which absorption occurs only at the donor, the MF should be "1," whereas the value of MF should be "−1" for the range in which absorption occurs only at the acceptor. Therefore, using the MF value, we can easily estimate the degree of energy-state matching at the interface between the donor and acceptor.

3.2 | Application of MF to two organic materials systems

The MF is applied to a two organic materials system based on a BHJ of the electron-donating conjugated polymer poly (4,8-bis(5-(2-ethylhexyl)thiophen-2-yl)benzo[1,2-b:4,5-b′] dithioph-ene-alt-4,6-bis(thieno[3,2-b]thiophen-5-yl)-5-octyl-2-(2-octyld-odecyl)pyrrolo[3,4-c]pyrrole-1,3(2H,5H)-dione)

(P1) and the electron-accepting material $PC_{71}BM$.[34,35] Figure 2A,B shows the molecular structures and absorption spectra of P1 and $PC_{71}BM$. Energy diagrams of P1 and $PC_{71}BM$ are shown in Figure 2C. The ODs of P1 and $PC_{71}BM$ at different incident-photon energies are shown in Figure 2D. P1 exhibits the highest OD at 2.4 eV (black line), and $PC_{71}BM$ exhibits the peak OD at 2.5 eV (blue line). The OD of P1 is overlapped with that of $PC_{71}BM$ in the range of 2.0–4.0 eV, and the highest overlapping photon energy is nearly 2.5 eV. The vertical arrows in Figure 2D indicate arbitrary photon energy for excitation generation with a scale set at 2.5 eV, and they illustrate the corresponding OD intensities of both materials when irradiated by a photon with an energy of 2.5 eV. The OD values are 0.8 and 0.5 for P1 and $PC_{71}BM$, respectively.

Figure 2E shows the MODs of P1 and $PC_{71}BM$ calculated via the summation of the HOMO level and irradiated photon energy for each material. The HOMO levels of P1 and $PC_{71}BM$ are −5.41 and −5.90 eV, respectively. When the materials absorb an incident photon with an energy of 2.5 eV, as shown in Figure 2E, the electrons in P1 are excited to hot states, with an energy of −2.91 eV, from their HOMO levels (−5.41 eV). In contrast, the electrons in $PC_{71}BM$ are excited to an energy state of −3.4 eV from their HOMO levels (−5.9 eV). The yellow area in Figure 2E indicates the MODO area between P1 and $PC_{71}BM$, and this area significantly differs from that of the ODO in Figure 2D. The MOD of P1 is higher than that of $PC_{71}BM$ in the range between −2.75 and −3.4 eV, whereas that of $PC_{71}BM$ is higher above −2.75 eV and below −3.4 eV; the MODs of P1 and $PC_{71}BM$ are identical at −2.75 eV.

To visualize the amount of MODO, we calculated the MF for the BHJ of P1:$PC_{71}BM$. Figure 2F shows the calculated MF for P1:$PC_{71}BM$ (black line) at each energy

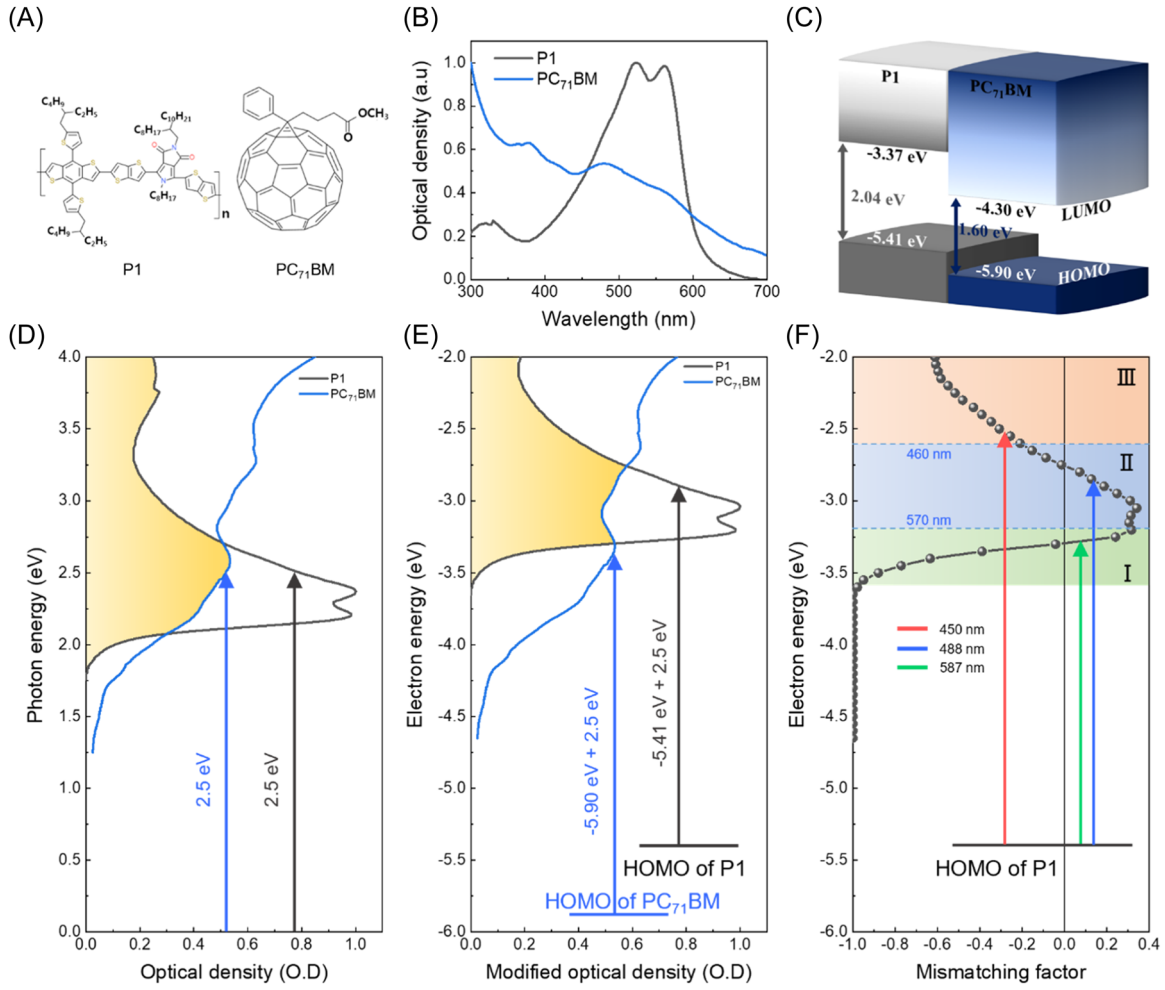

FIGURE 2 Material and optical properties of P1 and $PC_{71}BM$. (A) Molecular structures of P1 and $PC_{71}BM$. (B) Absorption spectra of P1 and $PC_{71}BM$. (C) Energy-level diagrams of P1 and $PC_{71}BM$. (D) OD of P1 and $PC_{71}BM$. (E) MOD of P1 and $PC_{71}BM$. (F) MF at the corresponding electron energy level for P1:$PC_{71}BM$.

level. The MF was calculated by subtracting $MOD_{acceptor}$ from MOD_{donor}, as described in Equation (2). The MFs are zero at −2.75 and −3.4 eV for P1:$PC_{71}BM$. However, the energy state at −3.4 eV lies near the LUMO level, where inefficient PICT easily occurs.[36] As previously explained, an MF of zero indicates that the amplitudes of the two MODs are equal and that the energy states at their interface are ideally matched. To derive an intuitive expression of the MF, we separated the range into three parts, as shown in Figure 2F, that is, Areas I, II, and III (green = Area I, blue = Area II, and red = Area III). Area I covers a deeper energy level than the hot state, which can be considered as the energy level with the highest MOD of the donor (−3.2 eV).[19,22] Therefore, although the state matching is good in Area I (such as −3.4 eV), the effect of energy matching is relatively small.[37] In contrast, Area III indicates the range where the value of MODO is under 0.4 (−2.6 eV), that is, an unbalanced energy level between the donor and acceptor. Using this approach, well-matched energy levels of P1:$PC_{71}BM$ with a small MF are obtained in Area II, where the intensities of the MODO are greater than 0.4, and the energy level is within the hot state. This value of 0.4 is selected based on the experimental results. In P1:$PC_{71}BM$, the excitation of electrons in Area II requires a photon energy of 460–570 nm, as shown in Figure 2F.

3.3 | Correlation between MF and V_{oc}

Because we expect that the Areas I, II, and III exhibit different PICT processes between P1 and $PC_{71}BM$, monochromatic light of different wavelengths (different photon energies) can be used to excite the electrons selectively to each state of the area.[38] Therefore, the correlation between the MODO and V_{oc} in the OPV device can be investigated by measuring the V_{oc} variation for the incident monochromatic light with different energy levels. Figure 3A shows the variation in the V_{oc} of the OPV device under irradiation of different monochromatic lights. The structure of the OPV device is shown in the inset of Figure 3A. Interestingly, the device exhibits noticeably different V_{oc} values upon irradiation with monochromatic light with different wavelengths. When monochromatic light with a wavelength of <455 nm was irradiated on the device, electrons were selectively excited to Area III due to incident energy absorption. Under irradiation with wavelengths of 350, 400, and 450 nm, the device exhibits a nearly constant V_{oc} of ~0.64 V. However, the higher V_{oc} from 0.64 to 0.72 V is observed when monochromatic light with a wavelength of ~480 nm is applied to the device. The higher V_{oc} is maintained under irradiation at wavelengths of 490 and 500 nm. The V_{oc} again decreases when the wavelength of

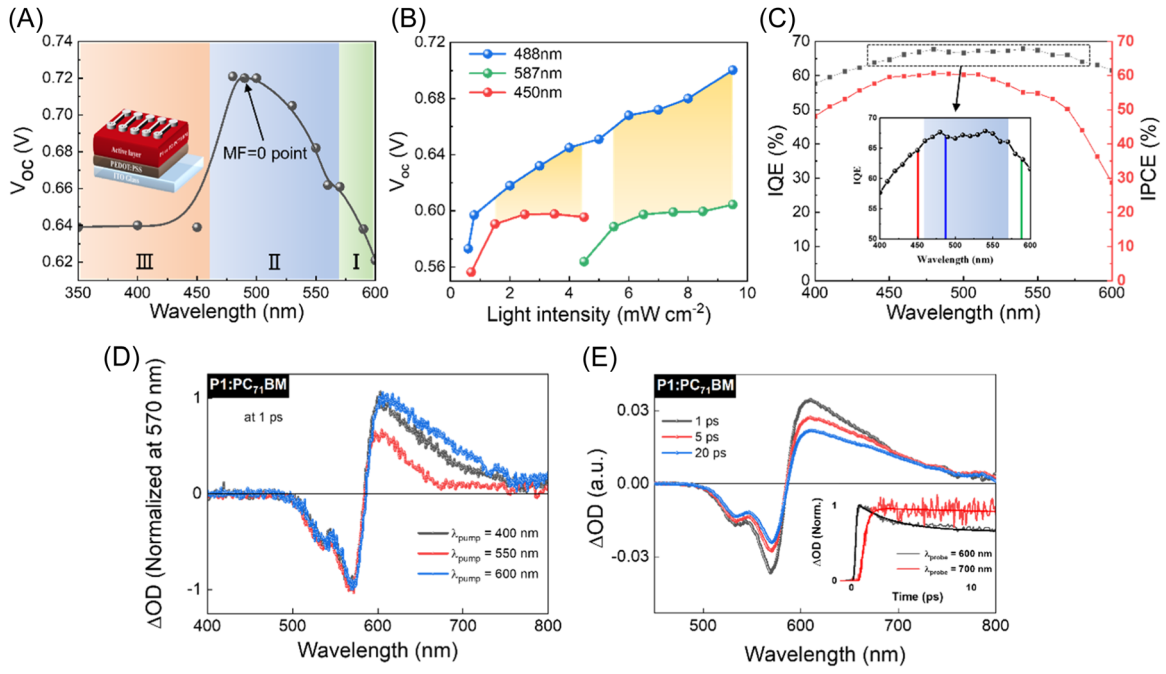

FIGURE 3 Correlation between MODO and V_{oc}. (A) Variations in the V_{oc} of P1:$PC_{71}BM$ irradiation by different wavelength. (B) Light-intensity-dependent V_{oc}. (C) IQE and IPCE of P1:$PC_{71}BM$. (D) TA spectra of the P1:$PC_{71}BM$ film were measured at 1 ps after pumping at 400, 550, and 600 nm; the spectra are normalized at 570 nm, and the pump intensity is 5 μJ cm^{-2}. (E) TA spectra of the P1:$PC_{71}BM$ film were obtained at 1, 5, and 20 ps using a pump wavelength of 600 nm; the pump intensity is 17 μJ cm^{-2}. The inset shows TA signal time decays probed at 600 and 700 nm.

the incident light exceeds 570 nm. However, the decrease in V_{oc} at 570 nm is also higher than those in Areas I and III. Because irradiation with wavelengths of 480–570 nm can excite electrons to Area II and irradiation with wavelengths larger than 570 nm can excite electrons to Area I, we can conclude that the excitation of electrons to Area II increases the V_{oc} of the device. Moreover, the highest V_{oc} is observed at the point where MF = 0.

This tendency is also observed in the variation of V_{oc} with an increase in the intensity of the monochromatic light, as shown in Figure 3B. We selected three monochromatic light wavelengths of 450, 488, and 587 nm, corresponding to the energy required to excite the electrons to Areas III, II, and I, respectively, and monitored the evolution of V_{oc} with the increasing light intensity. As shown in Figure 3B, the V_{oc} of the device irradiated by monochromatic light with wavelengths of 450 and 587 nm increases slightly with an increase in the light intensity and saturates at approximately 0.6 V. However, the V_{oc} of the same device under irradiation with monochromatic light of wavelength 488 nm continuously increases with the increasing light intensity from 0.6 to 9.5 mW cm^{-2}. Moreover, even when the irradiated light intensities are equal, a considerably high V_{oc} is obtained in case of light source of 488-nm wavelength. Because irradiation with monochromatic light of 488-nm wavelength excites the electrons to Area II with a well-matched energy state (MF = 0 at the point), these results clearly indicate that energy-level matching at the interface between the electron donor and acceptor is crucial for achieving a high V_{oc}. To examine the correlation between hot-state matching and the number of collected electrons, the internal quantum efficiency (IQE) and incident photon-to-current efficiency (IPCE) of the P1:$PC_{71}BM$ device were measured, and results are shown in Figure 3C. Although there is no correlation between the IPCE and MF, a high IQE is observed in Area II (blue area in the inset of Figure 3C). The red, blue, and green lines indicate 450, 488, and 587 nm, respectively. The IPCE in Area II is higher (> 65%) than those in Areas I and III. To verify our observations, we conducted the same experiment for the PTB7-Th:$PC_{71}BM$ BHJ, which is widely used in OPVs.[39] Figure S1 shows the (A) MODO, (B) MF of the PTB7-Th:$PC_{71}BM$ BHJ, and (C) the V_{oc} variations shown by the device. As expected, identical results are obtained for the PTB7-Th:$PC_{71}BM$ device, confirming our interpretation.

For further investigations, the transient absorption (TA) spectra and time-decay profiles of the P1 and P1:$PC_{71}BM$ films are measured (Figure S2). The P1 and P1:$PC_{71}BM$ films exhibit fast (~ 65 ps) and very long (> 2 ns) TA time-decay components, respectively, when they are pumped at 600 nm and probed at 565 (namely, photobleaching absorption regime) and 600 nm (namely, photoinduced absorption (PIA) regime). The approximately 65 ps component possibly results from fast relaxation from the singlet exciton state of P1, whereas the component larger than 2 ns component is indicative of an ultrafast and thus highly efficient electron transfer process from P1 to $PC_{71}BM$, and the generation of long-lived states of CT and polarons, as previously demonstrated in other fullerene-based BHJs.[18,40] To evaluate the effect of excitation wavelength on carrier dynamics, we measured the TA spectra of the P1:$PC_{71}BM$ film using three different pump wavelengths of 400, 550, and 600 nm (Figure 3D), which belong to the Areas III, II, and I, respectively. Compared to the TA spectra obtained using the pump wavelengths of 400 and 600 nm, the TA spectra obtained using the pump wavelength of 550 nm exhibit relatively low PIA spectral intensity at 600–700 nm. This shows that a well-matched energy level results in a reduced electron population in the CT states. To obtain more detailed information on the PIA spectra, we measured the TA spectra and time-decay profiles of the P1:$PC_{71}BM$ film using a high pump intensity of 17 μJ cm^{-2}, which may induce a carrier saturation at the CT states and a transition from the CT state to the polaron state (Figure 3E). As observed in the inset in Figure 3E, the fast (~ 3 ps) time-decay and (~ 2 ps) time-rise components at the probe wavelengths of 600 and 700 nm may be indicative of photoinduced CT and polaron bands at 600 and 700 nm, respectively, and a transition from the CT state to the polaron state. These results are in agreement with the previously reported results for other fullerene-based BHJs.[17,39] Following these PIA band assignments, the observed decrease in the PIA spectral intensity at 600–700 nm in the 550-nm pumped P1:$PC_{71}BM$ possibly indicates a reduction in the CT state population after photoexcitation, plausibly because of hot carrier transition. The reduced population in the CT states may decrease the V_{oc} loss in the OPVs.

3.4 | Estimation of V_{oc} loss in binary and ternary OPVs using the integration of MF

Because the V_{oc} of OPVs is highly sensitive to the MF value, which indicates the degree of state mismatching between the electron donor and acceptor in each energy level, the MF can be calculated to estimate the V_{oc} loss at the interface during PICT. A small absolute MF value indicates a high degree of energy-level matching (along with a high V_{oc} and small V_{oc} loss) and vice versa, as described in the definition of MF. However, because the donor material in an actual OPV device is excited by irradiation with an AM 1.5 solar light, with a wide spectral range, the electrons in the donor can be

simultaneously excited to Areas I, II, and III via solar-light absorption and then transferred to the acceptor via PICT. Therefore, the MF indicating the degree of energy matching at a specific energy state is insufficient to estimate the energy loss in an actual device under AM 1.5 solar-light irradiation.

For an actual OPV device irradiated by solar light, integrating each MF value (such as the yellow area of ③ in Figure 1C) for each energy state over the entire range of the MOD for the donor would be more useful. This integrated MF value is more meaningful than the individual MF values corresponding to each energy state, because the integration of the MF over the entire MOD range for the donor indicates the degree of MODO under solar-light irradiation. Figure 4A shows the correlation between V_{oc} and the integrated MF for P1:$PC_{71}BM$ and P2:$PC_{71}BM$. Because P1 and P2 have similar optical bandgaps (P1 = 2.04 eV, and P2 = 2.08 eV) and HOMO levels (P1 = −5.41 eV, and P2 = −5.44 eV) but different MOD shapes and MF values (see Figure S3A,B), a comparative analysis of these materials provides information for investigating the validity of the proposed MF integration method. The calculated integrated MF values for P1:$PC_{71}BM$ and P2:$PC_{71}BM$ are 0.452 and 0.440, respectively. As expected, the V_{oc} of P1:$PC_{71}BM$ is higher than that of P2:$PC_{71}BM$. This result was reproduced for PTB7-Th:$PC_{71}BM$, PTB7-Th:ITIC, and PTB7-Th:IEICO-4F, which are widely used as active materials in OPVs.[39,41] Figure 4B shows the variation in V_{oc} for the integrated MF values of these material compositions. All the device structures and fabrication processes were identical, except for the active materials. The integrated MF values of PTB7-Th:$PC_{71}BM$, PTB7-Th:ITIC, and PTB7-Th:IEICO-4F are 0.39, 0.36, and 0.45, respectively, and the resulting V_{oc} values are 0.78, 0.81, and 0.71 V, respectively. These results indicate that integrating the

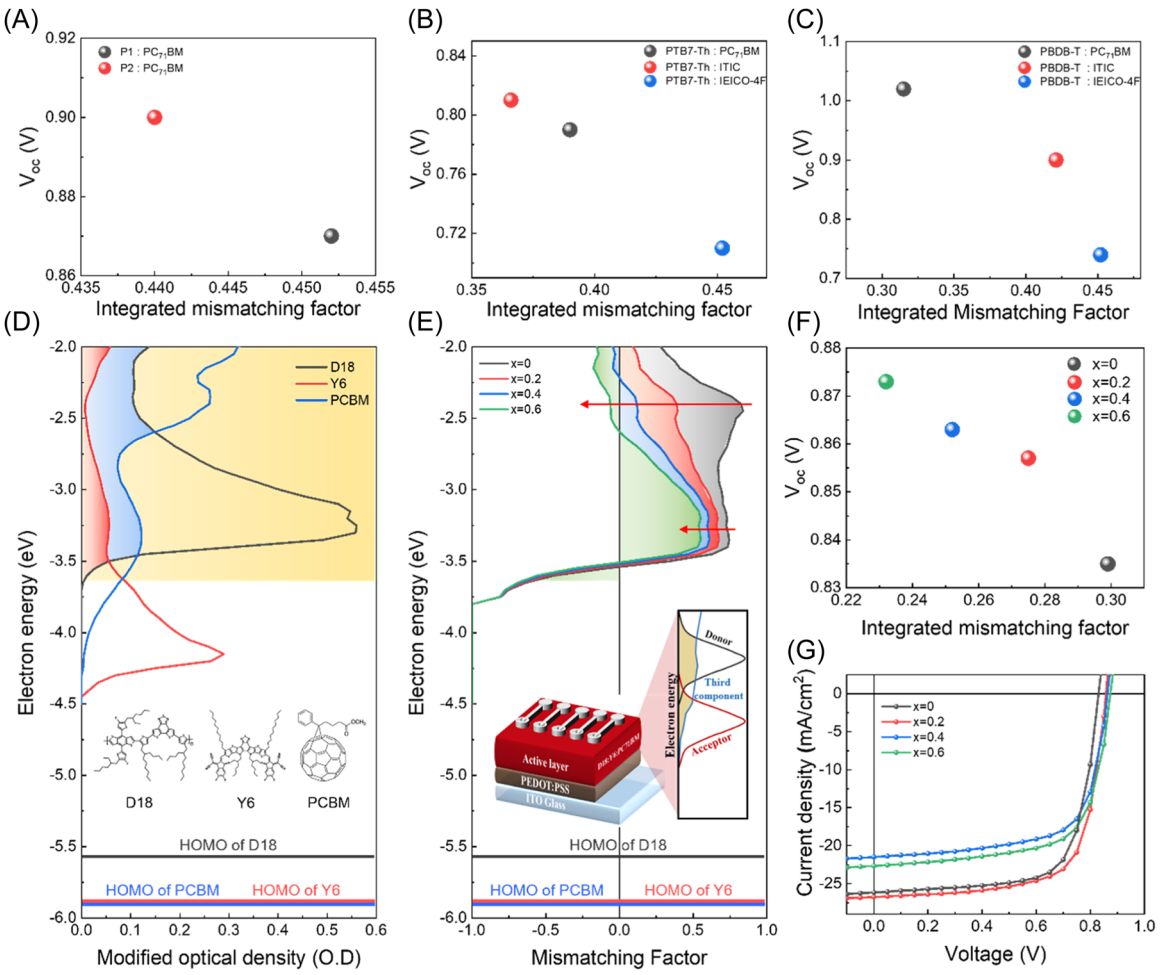

FIGURE 4 Photovoltaic properties for applying MODO to organic solar cells. (A) Integrated MF-dependent V_{oc} of P1:$PC_{71}BM$ and P2:$PC_{71}BM$. (B) Integrated MF-dependent V_{oc} of PTB7-Th-based photovoltaics. (C) Integrated MF-dependent V_{oc} of PBDB-T-based photovoltaics. (D) MOD of D18, Y6, and PCBM. (E) MF at each energy level of the D18:Y6:PCBM blended system. (F) Integrated MF-dependent V_{oc} with the ratio of the third component. (G) J–V characteristics for the optimized ratio of the third component. PCBM, phenyl-C61-butyric acid methyl ester.

MF value across the entire MOD range of the donor is a reasonable approach for estimating V_{oc} loss in OPVs. The relationship between integrated MF and V_{oc} is also observed in PBDB-T-based devices, as shown in Figure 4C.

To validate the concept of integrating MF into an actual device, we fabricated a ternary OPV device with three active materials. Because the absorbance of active materials can be changed by altering the ratio of the mixture in the ternary system, the MF value can be tuned by controlling the mixture ratio of these three materials.[42] For the ternary OPV device, D18 was selected as the donor material, and Y6 and PCBM were selected as the acceptors.[43] Although the MOD of D18 is considerably different from that of Y6, the MOD of PCBM covers the range of those of D18 and Y6 (see Figure 4D). Therefore, the MF of the ternary system can be tuned by controlling the amount of PCBM. The yellow box in Figure 4D indicates the integrated section of the integrated MF, and the red and blue areas indicate the MODO of D18:Y6 and D18:PCBM, respectively. Figure 4E shows the MF at each electron energy level of D18:Y6:PCBM, and the inset of Figure 4E shows the device structure along with the MODO of the donor, acceptor, and third component. The mass ratio of D18:Y6:PCBM was 1:1:x (where x represents the amount of PCBM and was set to 0, 0.2, 0.4, or 0.6). As shown in Figure 4E, the MF of the ternary system varies with the changing PCBM content. The red arrows around −2.4 eV indicate the MF variation caused by the addition of PCBM. The ternary system with 0.6 x value (green) exhibits an MF value of nearly zero at −2.5 eV, indicating a high degree of MODO between the D18 donor and Y6 and PCBM acceptors at −2.5 eV. The integrated MFs of the ternary system, when $x = 0.6$, 0.4, 0.2, and 0, are 0.232, 0.252, 0.275, and 0.299, respectively. Figure 4F presents the variations in V_{oc} at different values of the integrated MF and indicates that large integrated MF values correspond to low V_{oc} values. The highest V_{oc} is observed when $x = 0.6$, which corresponds to the smallest integrated MF of 0.232.

Figure 4G shows the current–voltage (J–V) curves of the ternary devices with different mixture ratios. OPV devices exhibit advantageous short-circuit current density (J_{sc}), V_{oc}, and fill factor (FF) values, which are conducive to their high performances. The J_{sc} and V_{oc} vary with the changing mixture ratio of the ternary system, as shown in Table 1. The highest PCE of 16.15% is observed for a device with a D18:Y6:PCBM ratio of 1:1:0.2, whereas the highest V_{oc} is observed for a device with a D18:Y6:PCBM ratio of 1:1:0.6. Because the PCE is determined by the J_{sc}, FF, and V_{oc}, the optimal mixing ratio for maximizing the V_{oc} slightly differs from that for maximizing the PCE; this difference can be overcome by optimizing the nanoscale morphology of the active layer. To verify the correlation between V_{oc} and MF, we fabricated ternary OPVs using PBDB-T, ITIC, and $PC_{71}BM$ and conducted the same experiments. Figure S4 presents the (A) MFs, (B) V_{oc} variations, and (C) J–V curves of the PBDB-T:ITIC:$PC_{71}BM$ ternary devices. The experimental results shown in Figure S4 agree well with those of the D18:Y6:PCBM ternary devices. The V_{oc} of OPVs is often predicted using an empirical rule ($qV_{oc} = E_g - 0.3$ eV). However, the value obtained using this empirical rule is different from those of the actual devices owing to various factors (induced gap tail states, carrier mobility, and morphology). Conversely, the MF-based method developed in this study is a derivation technique based on the absolute spectrum of the final coated thin film. This MF-based method encompasses the factors mentioned earlier and can thus be used to predict V_{oc} for an actual device using a simple process. Therefore, we can conclude that the integrated MF can be used to estimate the V_{oc} loss at the interface during PICT.

TABLE 1 Photovoltaic properties of D18:Y6:PCBM blend with various ratio.

Ratio (D18:Y6:PCBM)	MF	J_{sc} (mA cm^{-2})	V_{oc} (V)	FF	PCE (%)
1:1:0	0.299	26.15	0.83	0.69	15.29
1:1:0.2	0.275	26.75	0.85	0.70	16.15
1:1:0.4	0.252	21.49	0.86	0.67	12.56
1:1:0.6	0.232	22.68	0.87	0.67	13.37

Abbreviations: FF, fill factor; MF, mismatching factor; PCBM, phenyl-C61-butyric acid methyl ester; PCE, power conversion efficiency.

4 | CONCLUSION

We developed an effective method to quantify the degree of hot-state matching between donors and acceptors in OPVs. In this method, the MF of the BHJ thin film is determined from the MODO between the donor and acceptor to identify the degree of the energy-state mismatch between the electron donor and acceptor at their interface. A small MF value indicates a high degree of energy-level matching, whereas a large MF value indicates a low degree of state overlapping at the BHJ interface. Using the MF value, we evaluated the correlation between the V_{oc} loss of the OPVs and the energy-state matching at the BHJ interface. In binary systems, OPVs with small MFs exhibit high V_{oc} values,

and this tendency has been confirmed for ternary OPV devices with three active materials. Based on these results, we can conclude that energy-state matching between donors and acceptors is critical for reducing energy loss and maximizing V_{oc}. Finally, we achieved a high-efficiency ternary OPV device with a PCE of 16.15% by controlling the MF value. We believe that the MF determined in this study enables the estimation of V_{oc} loss in OPVs and allows the designing of optimized mixtures of donors and acceptors for high-performance OPV devices with a maximum V_{oc}.

ACKNOWLEDGMENTS

This research was supported by the BrainLink Program (2022H1D3A3A01077343) and the Nano Material Technology Development Program (2021M3H4A1A02057007) funded by the Ministry of Science and ICT through the National Research Foundation of Korea. This research was also supported by the Basic Science Research Program through NRF funded by the Ministry of Education (2022R1A6A1A03051158).

CONFLICT OF INTEREST STATEMENT

The authors declare that there are no conflicts of interests.

ORCID

Hyun-Seock Yang https://orcid.org/0009-0009-1876-2461
In-Wook Hwang https://orcid.org/0000-0002-9314-2598

REFERENCES

1. Hou J, Inganäs O, Friend RH, Gao F. Organic solar cells based on non-fullerene acceptors. *Nat Mater*. 2018;17(2):119-128.
2. Kirchartz T, Rau U. What makes a good solar cell? *Adv Energy Mater*. 2018;8(28):1703385.
3. Dennler G, Scharber MC, Brabec CJ. Polymer-fullerene bulk-heterojunction solar cells. *Adv Mater*. 2009;21(13):1323-1338.
4. Menke SM, Ran NA, Bazan GC, Friend RH. Understanding energy loss in organic solar cells: toward a new efficiency regime. *Joule*. 2018;2(1):25-35.
5. Ma X, Wang J, Gao J, et al. Achieving 17.4% efficiency of ternary organic photovoltaics with two well-compatible nonfullerene acceptors for minimizing energy loss. *Adv Energy Mater*. 2020;10(31):2001404.
6. Zhang L, Zhang Z, Deng D, Zhou H, Zhang J, Wei Z. "N–π–N" type oligomeric acceptor achieves an OPV efficiency of 18.19% with low energy loss and excellent stability. *Adv Sci*. 2022;9(23):2202513.
7. Yan Y, Zhang Y, Liu Y, et al. Simultaneously decreasing the bandgap and V_{oc} loss in efficient ternary organic solar cells. *Adv Energy Mater*. 2022;12(20):2200129.
8. Izawa S, Shintaku N, Kikuchi M, Hiramoto M. Importance of interfacial crystallinity to reduce open-circuit voltage loss in organic solar cells. *Appl Phys Lett*. 2019;115(15):153301.
9. Gregg BA, Hanna MC. Comparing organic to inorganic photovoltaic cells: theory, experiment, and simulation. *J Appl Phys*. 2003;93(6):3605-3614.
10. Veldman D, Meskers SCJ, Janssen RAJ. The energy of charge-transfer states in electron donor-acceptor blends: insight into the energy losses in organic solar cells. *Adv Funct Mater*. 2009;19(12):1939-1948.
11. Bakulin AA, Rao A, Pavelyev VG, et al. The role of driving energy and delocalized states for charge separation in organic semiconductors. *Science*. 2012;335(6074):1340-1344.
12. Liu S, Yuan J, Deng W, et al. High-efficiency organic solar cells with low non-radiative recombination loss and low energetic disorder. *Nat Photonics*. 2020;14(5):300-305.
13. Janssen RAJ, Nelson J. Factors limiting device efficiency in organic photovoltaics. *Adv Mater*. 2013;25(13):1847-1858.
14. Wei M, Wang Z, Wen Z, Hao X, Qin W. Utilizing magnetic field to study the impact of intramolecular charge transfers on the open-circuit voltage of organic solar cells. *Appl Phys Lett*. 2018;113(9):093301.
15. Wang Y, Zhou L, Zhang C, et al. Conjugated starbursts with acceptor–π–donor–π–acceptor architectures as nonfullerene acceptors for high-efficiency organic solar cells. *J Phys Chem C*. 2022;126(46):19594-19602.
16. Li X, Wang H, Nakayama H, et al. Multi-sulfur-annulated fused perylene diimides for organic solar cells with low open-circuit voltage loss. *ACS Appl Energy Mater*. 2019;2(5):3805-3814.
17. Gong Y, Kan Z, Xu W, et al. Wide-bandgap small molecular acceptors based on a weak electron-withdrawing moiety for efficient polymer solar cells. *Solar RRL*. 2018;2(10):1800120.
18. Hwang IW, Soci C, Moses D, et al. Ultrafast electron transfer and decay dynamics in a small band gap bulk heterojunction material. *Adv Mater*. 2007;19(17):2307-2312.
19. Jakowetz AC, Böhm ML, Zhang J, et al. What controls the rate of ultrafast charge transfer and charge separation efficiency in organic photovoltaic blends. *J Am Chem Soc*. 2016;138(36):11672-11679.
20. Grancini G, Maiuri M, Fazzi D, et al. Hot exciton dissociation in polymer solar cells. *Nat Mater*. 2013;12(1):29-33.
21. Jailaubekov AE, Willard AP, Tritsch JR, et al. Hot charge-transfer excitons set the time limit for charge separation at donor/acceptor interfaces in organic photovoltaics. *Nat Mater*. 2013;12(1):66-73.
22. Tamura H, Burghardt I. Ultrafast charge separation in organic photovoltaics enhanced by charge delocalization and vibronically hot exciton dissociation. *J Am Chem Soc*. 2013;135(44):16364-16367.
23. Grantham-McGregor SM, Powell CA, Walker SP, Himes JH. Role for human capital policies? *Proc Natl Acad Sci USA*. 1979;163(2):411-416.
24. Zheng Z, Tummala NR, Fu YT, Coropceanu V, Brédas JL. Charge-transfer states in organic solar cells: understanding the impact of polarization, delocalization, and disorder. *ACS Appl Mater Interfaces*. 2017;9(21):18095-18102.
25. Heeger AJ. 25th Anniversary article: bulk heterojunction solar cells: understanding the mechanism of operation. *Adv Mater*. 2014;26(1):10-28.
26. Tamura H, Burghardt I. Potential barrier and excess energy for electron-hole separation from the charge-transfer exciton at

donor-acceptor heterojunctions of organic solar cells. *J Phys Chem C*. 2013;117(29):15020-15025.
27. Rao A, Chow PCY, Gélinas S, et al. The role of spin in the kinetic control of recombination in organic photovoltaics. *Nature*. 2013;500(7463):435-439.
28. Wang ZS, Sha WEI, Choy WCH. Exciton delocalization incorporated drift-diffusion model for bulk-heterojunction organic solar cells. *J Appl Phys*. 2016;120(21):213101.
29. Boström EV, Mikkelsen A, Verdozzi C, Perfetto E, Stefanucci G. Charge separation in donor-C60 complexes with real-time green functions: the importance of nonlocal correlations. *Nano Lett*. 2018;18(2):785-792.
30. Brigeman AN, Fusella MA, Yan Y, et al. Revealing the full charge transfer state absorption spectrum of organic solar cells. *Adv Energy Mater*. 2016;6(21):1601001.
31. Vandewal K, Albrecht S, Hoke ET, et al. Efficient charge generation by relaxed charge-transfer states at organic interfaces. *Nat Mater*. 2014;13(1):63-68.
32. Burke TM, Sweetnam S, Vandewal K, McGehee MD. Beyond Langevin recombination: how equilibrium between free carriers and charge transfer states determines the open-circuit voltage of organic solar cells. *Adv Energy Mater*. 2015;5(11):1500123.
33. Bertrandie J, Han J, De Castro CSP, et al. The energy level conundrum of organic semiconductors in solar cells. *Adv Mater*. 2022;34(35):2202575.
34. Tamilavan V, Kim S, Sung JY, et al. Effects of the incorporation of bithiophene instead of thiophene between the pyrrolo[3,4-c]pyrrole-1,3-dione units of a bis(pyrrolo[3,4-c]pyrrole-1,3-dione)-based polymer for polymer solar cells. *New J Chem*. 2016;40(12):10153-10160.
35. Tamilavan V, Lee J, Agneeswari R, et al. Efficient pyrrolo[3,4-c]pyrrole-1,3-dione-based wide band gap polymer for high-efficiency binary and ternary solar cells. *Polymer*. 2017;125:182-189.
36. Khan SUZ, Gui M, Liu X, Giebink NC, Kahn A, Rand BP. Nonradiative recombination via charge-transfer-exciton to polaron energy transfer limits photocurrent in organic solar cells. *Adv Energy Mater*. 2022;12(19):2200551.
37. Jungbluth A, Kaienburg P, Riede M. Charge transfer state characterization and voltage losses of organic solar cells. *J Phys Mater*. 2022;5(2):024002.
38. Yao Y, Xie X, Ma H. Ultrafast long-range charge separation in organic photovoltaics: promotion by off-diagonal vibronic couplings and entropy increase. *J Phys Chem Lett*. 2016;7(23):4830-4835.
39. Wan Q, Guo X, Wang Z, et al. 10.8% Efficiency polymer solar cells based on PTB7-Th and $PC_{71}BM$ via binary solvent additives treatment. *Adv Funct Mater*. 2016;26(36):6635-6640.
40. Hwang IW, Cho S, Kim JY, et al. Carrier generation and transport in bulk heterojunction films processed with 1,8-octanedithiol as a processing additive. *J Appl Phys*. 2008;104(3):033706.
41. Lin Y, Wang J, Zhang ZG, et al. An electron acceptor challenging fullerenes for efficient polymer solar cells. *Adv Mater*. 2015;27(7):1170-1174.
42. Lee J, Tamilavan V, Rho KH, et al. Overcoming fill factor reduction in ternary polymer solar cells by matching the highest occupied molecular orbital energy levels of donor polymers. *Adv Energy Mater*. 2018;8(9):1702251.
43. Qin J, Zhang L, Xiao Z, et al. Over 16% efficiency from thick-film organic solar cells. *Sci Bull*. 2020;65(23):1979-1982.

SUPPORTING INFORMATION

Additional supporting information can be found online in the Supporting Information section at the end of this article.

How to cite this article: Yang H-S, Kim D, Oh C-M, et al. Understanding the correlation between energy-state mismatching and open-circuit voltage loss in bulk heterojunction solar cells. *Carbon Energy*. 2024;6:e433. doi:10.1002/cey2.433